The use of supercritical water for the catalyst-free oxidation of coarse aluminum for hydrogen production

Keena A. Trowell[a],*, Sam Goroshin[a],
David L. Frost[a], Jeffrey M. Bergthorson[a]

[a] Alternative Fuels Laboratory, Department of Mechanical Engineering, McGill University, Canada

Abstract

Maximizing the use of renewable resources requires clean, sustainable and recyclable energy carriers for energy trade and long-term storage. Aluminum is energy dense, plentiful, recyclable and, when reacted with water, the stored energy is released as hydrogen and heat. In this study, we investigated the use of high-temperature liquid water and supercritical water as oxidizers for coarse aluminum. We performed experiments using a variety of aluminum morphologies, including coarse aluminum pieces measuring up to 3 mm in diameter, and water ranging in temperature from 475 K to 650 K (and the corresponding saturated vapour pressures). Previous studies of aluminum-water reactions have focused on low temperature experiments using catalysts, specialized alloys, or nano-powders to increase reaction efficiency. These low-temperature approaches have been shown to be effective but add complexity, expense, and waste the thermal energy of the reaction.

Our results show that, without special measures, 100 % hydrogen yield is possible from coarse aluminum particles, and scrap aluminum, when reaction temperature and pressure are increased. A change in reaction efficiency was observed at 550 K. Up to this temperature, the 55 µm and 120 µm powders had yields below 30 %, the aluminum slugs and 2 mm plate had a yields close to zero. At temperatures between 550 K and the supercritical temperature, there was a marked increase in hydrogen yield. At temperatures above 647 K and pressures above 220 bar, the critical point of water, 100 % of the theoretical hydrogen yield was achieved across all samples tested. These findings open the door to using aluminum as a recyclable energy carrier for renewable energy.

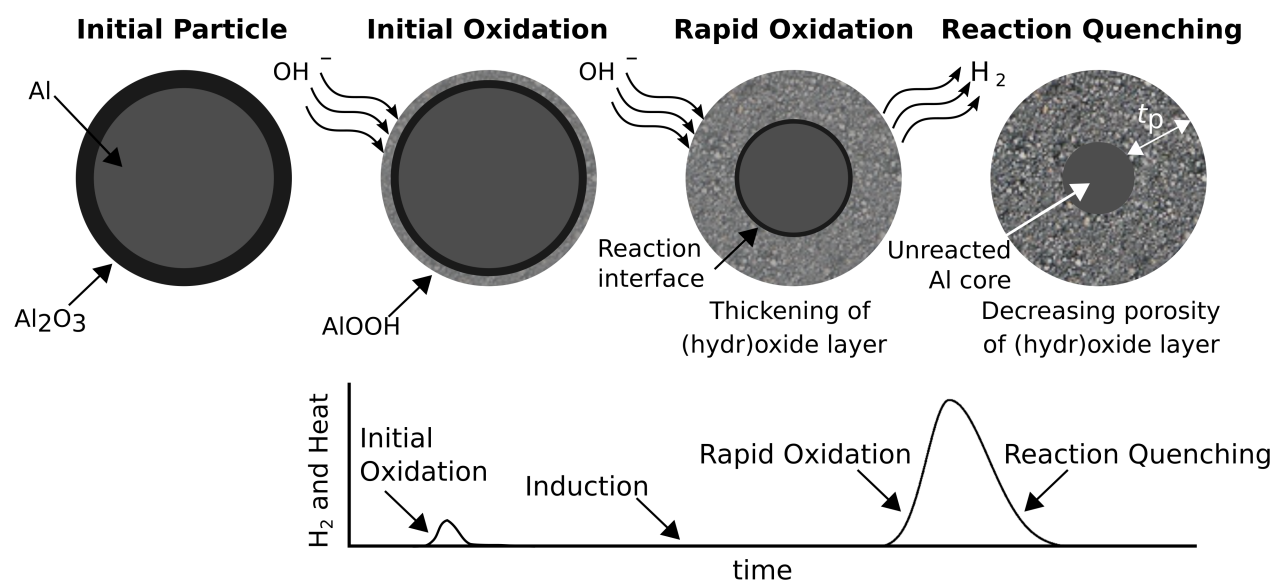*Corresponding author: keena.trowell@mail.mcgill.ca

Figure 1: Aluminum-water reaction phases. An initial oxidation is followed by an induction period during which the aluminum oxide passivation layer is hydrated and weakened. Once the passivation layer is sufficiently weakened, rapid oxidation takes place and continues until the formed hydroxides quench the reaction, potentially leaving an unreacted aluminum core and resulting in lower yields. The thickness of the formed oxide layer, or penetration thickness, is denoted as t_{p}. Adapted from Bergthorson et al.[2]

1   Background

The continued use of hydrocarbons is untenable as the effects of climate change take hold. A complete shift towards renewable power generation is necessary, and, for this shift to take place, sustainable energy carriers are required. These energy carriers will be the mechanism by which renewable energy can be commodified. The commodification of renewable energy will allow for global trade and seasonal storage of clean energy, two key aspects to managing the geographical and seasonal variability of renewable resources.[1] These energy carriers may also replace hydrocarbon fuels, particularly in applications which require sustained high power, such as long-distance marine and land transport.

1.1   Aluminum as an energy carrier

A metal-fuel cycle has been proposed wherein metals, processed using clean energy, are used as energy carriers.[2] The energy dense metals are safer and more convenient to store and transport than hydrogen. The metal oxide products, which are inert and non-toxic, can be recycled, again, using clean energy.[3]
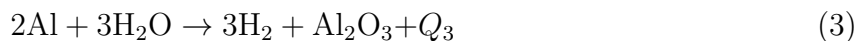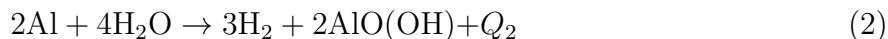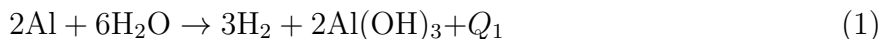
Aluminum is particularly well-suited to fill the role of a sustainable energy carrier because it has a specific energy, one comparable to hydrocarbons (E_{al}= 31 MJ/kg).[1] Aluminum is also abundant and the technology for producing aluminum without GHG emissions is on the horizon.[4,5] Aluminum, produced *via* electrolysis requires approximately 50 MJ per kilogram,[6] thus has an electricity-to-fuel efficiency comparable to hydrogen production *via* electrolysis

of around 60%.[7,8] However, aluminum as an energy carrier offers several advantages over hydrogen in terms of safety, convenience and energetic losses during storage. The energy stored in aluminum can then be released through direct combustion in air,[9] or through reaction with water to release heat and hydrogen.[10–14]

1.2 Aluminum-water reactions

When reacted with water, about half of the energy stored in aluminum evolves as hydrogen and, due to the highly exothermic nature of aluminum-water reactions, the other half of the reaction energy evolves as heat. Aluminum has a fairly high volumetric hydrogen yield of 1.2 L per gram of aluminum.[14,15] When the aluminum-water reaction occurs at high temperature, the reaction produces high-quality heat which can be used for power.[10] The hydrogen produced by the reaction may be fed to a fuel cell,[11,16–18] or combusted in air to power a turbine or a heat engine.[10] In addition to power generation,[17,19,20] aluminum-water systems have also been studied for use as green propellants,[21,22] and for underwater propulsion.[23,24] On demand, *in-situ* hydrogen production, through the reaction of aluminum with water, would allow for the use of hydrogen while avoiding the safety concerns.

The reaction proceeds in four phases,[25] as illustrated in Fig. 1, because of the presence of a passivating layer of amorphous alumina on the surface of the aluminum.[27] A weak, quickly quenched, initial oxidation phase takes place during the first few minutes of contact between the reactants and is followed by an induction phase wherein hydrolysis of the passivating oxide takes place.[25–28] Once the passivating oxide has been adequately compromised, rapid evolution of hydrogen gas and heat occurs. Finally, the reaction is quenched as a result of the formation of tenacious hydroxides. The aluminum-water reaction follows one of three reaction pathways, shown as Eqs. 1, 2, 3. All three pathways result in the same ratio of formed hydrogen gas to aluminum but the stoichiometric amount of water changes.[29] It has been reported that the thermodynamically preferred pathway is a function of temperature,[26] but this conflicts with experimentally observed results[27,30–32] and neglects the effect of pressure. The thermal products of reaction, $Q_{n=1,2,3}$, which vary as a function of temperature and pressure,[31] are on the order of 400–450 kJ per mol of aluminum.[31]

$$2Al + 6H_2O \rightarrow 3H_2 + 2Al(OH)_3 + Q_1 \tag{1}$$

$$2Al + 4H_2O \rightarrow 3H_2 + 2AlO(OH) + Q_2 \tag{2}$$

$$2Al + 3H_2O \rightarrow 3H_2 + Al_2O_3 + Q_3 \tag{3}$$

1.3 Catalyzed aluminum-water reactions

Research in the field has largely focused on enhancing reaction efficiency by compromising the protective amorphous oxide layer. The use of alkalis,[33–35] alloys or dopants,[36–38] increased specific surface area (by using nanoparticles),[25,39] and mechanical manipulation of powders[40–42] or the surface[43] have been tested. These approaches have been, to various degrees, successful in increasing reaction rates and yields; however, drawbacks include increased complexity, increased expense, formation of corrosive reaction products, and lower reaction onset temperatures.[10] The low reaction onset temperature, in some cases as low as

3

300 K, has two major drawbacks. First are the safety implications due to the the risk of accidental oxidation by water. Secondly, as approximately half of the energy of the reaction evolves as heat, the heat evolved in a low-temperature reaction is low-quality heat which cannot be used for work. These low-temperature approaches effectively waste half of the energy content of the aluminum and require very fine powders to achieve full oxidation.

1.4 High-temperature aluminum-water reactions

The use of coarser particles in an aluminum-water power system is desirable for a variety of reasons. Larger particles have a higher specific fuel content, are less expensive to produce, and are safer to store, transport and handle because the risk of premature oxidation is minimal. However, achieving complete oxidation using coarse particles is a major challenge. Full reaction of larger particles is limited by the formation of the hydroxide reaction products. These hydroxides slow the reaction by impeding the migration of hydroxyl ions to the reaction interface,[25–28] potentially leaving an unreacted aluminum core, as shown in Fig. 1. This unreacted core is effectively wasted fuel.

Earlier work has shown that although an increase in reaction temperature leads to an increase in reaction completeness,[13,44,45] the penetration thickness, the difference between initial particle radius and the radius of the unreacted core following reaction, labelled t_p in Fig. 1, is independent of particle size.[13] This implies that, at each temperature, there is an upper limit to the particle size with which full hydrogen yield can be achieved. This also implies that it should be impossible to fully oxidize larger particles using liquid water. It should be noted, however, that Yavor's study was limited to temperatures below 475 K and to pure aluminum powders no larger than 12 µm.

Our novel approach uses supercritical water to create an efficient oxidation regime for aluminum. We expect that supercritical water, which can dissolve non-polar species, would prevent the formation of a cohesive hydroxide layer, the mechanism which normally prevents complete oxidation. In this work, we use high-temperature and high-pressure liquid water and supercritical water as an oxidizer, with temperatures ranging from 475 K to 650 K. No addition of catalysts or other reaction enhancement methods is employed. In our experiments, we use a variety of pure aluminum powders, slugs, and plates, as well as a shredded aluminum can, as fuel.

2 Experimental Procedures

A purpose-built apparatus, shown in Fig. 2, was used to conduct the experiments in this study. The central component of the experimental apparatus is a GC-1 high-pressure confined-gasket-closure reactor manufactured by High Pressure Equipment Company (USA), chosen because it is designed to hold the pressures and temperatures required in this work. An aluminum mantle was machined to house the reactor. A 1250 W resistance heater was placed over the mantle to supply heat to the reactor during experiments. At the end of each experiment, cold water flows through a series of channels in the mantle to cool the system to room temperature. A dual-output K-type thermocouple (Omega CAXL-116-U-12-DUAL) and a pressure transducer (WIKA A-10) are used to monitor the conditions inside the reactor. One output of the thermocouple is connected to a temperature controller, the other
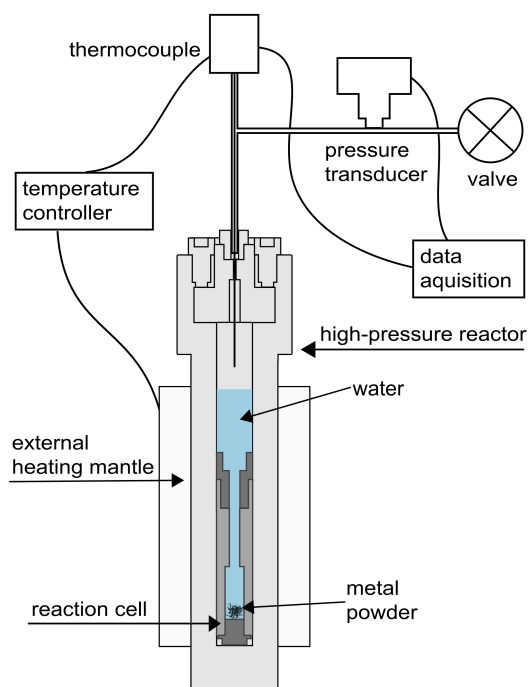
4

Figure 2: Schematic of apparatus. A measured amount of aluminum powder is placed in the crucible of the reaction cell. The cell is then placed in the reactor, and a measured amount of water is poured into the reactor, which is then sealed and heated to the temperature of interest. The pressure and temperature readings are recorded by the data acquisition system.
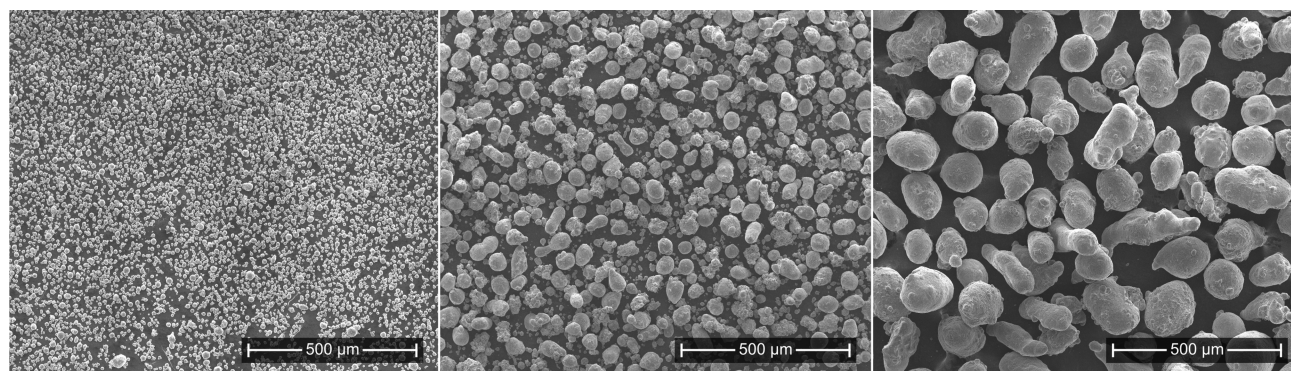
Figure 3: SEM of powders, as received. Aluminum powders are shown at 100x magnification. (left) $12\,\mu m$, (center) 55 μm, (right) $120\,\mu m$.

thermocouple output, as well as the pressure transducer, are connected to a Raspberry Pi computer. The Pi is equipped with an analogue to digital converter chip (MCP3008) and a thermocouple amplifier chip (MAX31855). The data from the thermocouple and pressure transducer is recorded using a code written in Python 2.7.

Three micron-scale aluminum powders were used in the present work along with coarse aluminum slugs, plates, and remnants of common aluminum cans. The three powders have a nominal diameter of $12\,\mu m$, $55\,\mu m$, and $120\,\mu m$, respectively. Documentation from the supplier, Valimet (Stockton, California) state that these powders are 99.7% pure aluminum and have no coating other than the naturally occurring passivation layer of aluminum oxide on the surface of the powder. Scanning electron microscope (SEM) images of the three powders are shown in Fig. 3. The aluminum slugs and plates used in this work are 99.99% pure and were obtained from Alfa Aesar. The 2mm-thick plate was cut to pieces measuring approximately 10 mm by 100 mm. The cutting was done in the lab using tin snips and was only done to ease loading into the reactor.

Common aluminum beverage cans (LaCroix brand and Pepsi brand) were used in this work. The can wall was separated from the top and only samples from the wall section were used. In one set of experiments, no attempt was made to remove brand markings on the can, or any of its interior or exterior coatings. In another set of experiments, the can was sanded with 220 grit sandpaper until the brand markings on the outside were removed. The interior was also sanded in order to remove the protective polymer coating. In each case, the aluminum can was cut into pieces measuring approximately 3 mm by 25 mm.

A measured amount of aluminum and deionized water is placed inside the reactor cell before the reactor is sealed. Approximately 1 g of aluminum and 27 ml of deionized water are used in each experiment. The amount of water is much higher than the stoichiometric amount of 1 gram (or 1 mL at STP) of water per gram of aluminum. The amount of water is calibrated to prevent complete boil off thereby ensuring that, at temperatures below the critical temperature (T_c), liquid water is always present. This amount of water also ensures the density of the water is equal to the critical density when the system is at the critical temperature. Once the reactor is sealed, the initial pressure, p_1, is recorded.

The sealed reactor is heated to the desired temperature and held at that temperature for 30 minutes. The reactor pressure is equal to the vapor pressure, even as hydrogen evolves,

because of hydrogen's ability to dissolve into high-temperature water.[46] The system is then cooled to the initial temperature and a final pressure value, p_2, is recorded. The hydrogen yield of the reaction in moles, n_{H_2}, is determined by comparing the initial pressure to the final pressure using the ideal gas law:

$$n_{H_2} = \frac{(p_2 - p_1)V}{RT} \tag{4}$$

where V is the free volume inside the apparatus [ml], R is the universal gas constant [ml·bar/mol·K] and T is temperature in Kelvin. Moles of hydrogen are then converted to mL of hydrogen at standard temperature and pressure (STP) and reported as a percentage of full yield, which is 1200 ml per gram of aluminum.
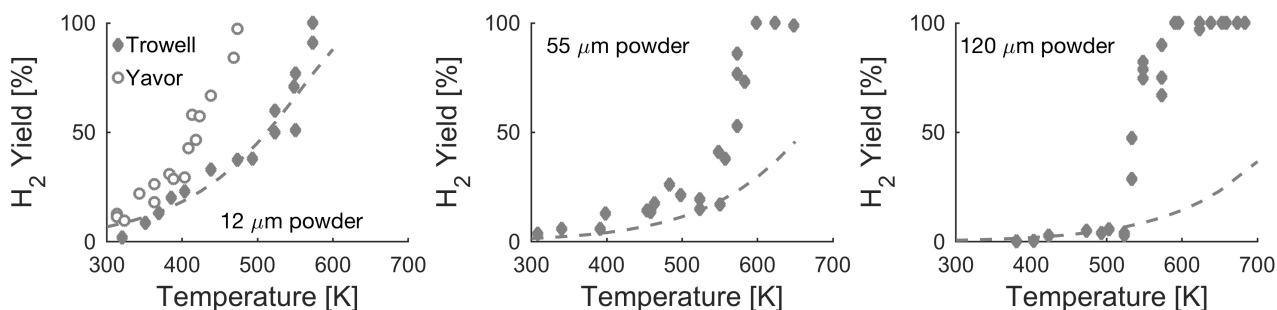
3   Results

Figure 4: Hydrogen yield of each aluminum powder. Hydrogen yield is reported as a percentage of the full yield of approximately 1200 ml of hydrogen per gram of aluminum. The diamond markers denote the measured results from this work and the circle markers denote the results from Yavor *et al.*[13] The dashed line illustrates the expected yield based on Yavor's hypothesis that penetration thickness is independent of particle size. In the case of the 55 μm and 120 μm powder, the actual yield is significantly higher than the predicted yield for temperatures above 550 K.
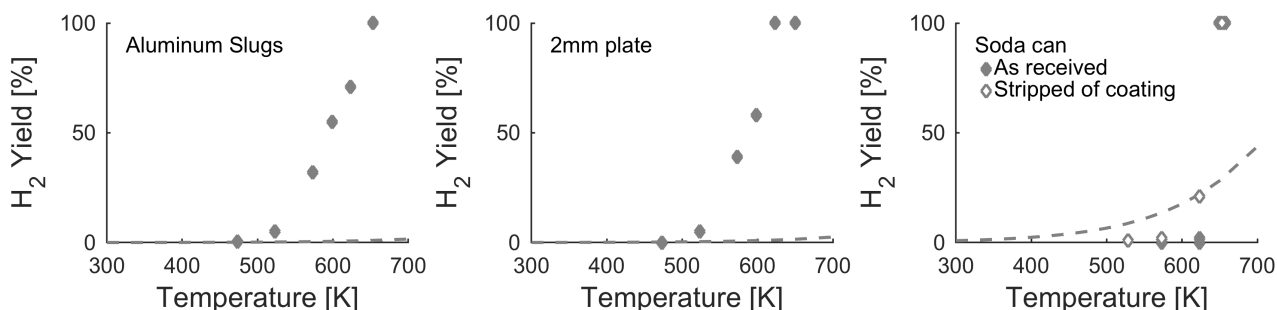

Figure 5: Hydrogen yield of aluminum slugs, plates, and common aluminum beverage can. The dashed line indicates the expected yield and the diamond markers show the measured yield. No significant reaction onset occurs before 525 K and full oxidation is achieved in supercritical water.

3.1 Reaction efficiency in a pre-mixed vs pre-heat regime

The reaction efficiency as a function of reaction temperature is shown in Fig. 4. The first panel shows the results using a 12 μm powder under two experimental regimes. The filled diamond markers are the results from this work, wherein the reactants are pre-mixed and heated to temperature together. The open circles are the results from work done by Yavor *et al.*[13] where the reactants were pre-heated separately then rapidly mixed once the system reached the desired temperature. Up to 400 K, there is very little difference between the results of the two sets of experiments but, as the temperature increases, the difference in yield between the two studies increases. Full conversion is achieved in both cases but Yavor *et al.* achieved full yield at 450 K, while in our work we achieve it at 550 K.

We attribute the lower reaction efficiency of the present pre-mixed experiments to the decreased porosity of the formed hydroxide. Two competing processes occur during the induction phase: hydrolysis of the existing passivating layer of amorphous aluminum oxide, and formation of crystalline hydroxides. The crystalline hydroxides slow the reaction, but are themselves slow to form because the crystallization occurs through a dissolution-precipitation process.[27] Rapid oxidation occurs once the rate of hydrolysis exceeds the rate of the crystalline hydroxide formation.

In the pre-mixed experiments, rapid oxidation begins at the lowest temperature at which the rate of hydrolysis of the alumina layer outpaces the formation of new hydroxides. The relatively slow heating of the system allows time for the formed hydroxides to increase in density and prevent further oxidation at a given temperature. In the pre-heated experiments, the aluminum comes into contact with high-temperature water. We hypothesise that the oxidation rate at the elevated temperatures outpaces the rate at which the porosity diminishes, which results in a higher evolution of gaseous hydrogen at a given temperature.

Yavor *et al.*[13] hypothesized that the penetration thickness is independent of particle size. To test this hypothesis, we fit an exponential curve to the 12 μm data up to 475 K, which was the upper limit of their experiments. We chose to fit only the portion of our data which overlapped with the particle size and temperature range studied by Yavor *et al.* in order to understand if their findings could be generalized to other temperatures and powders. This curve was then extrapolated to higher temperatures and the other powder sizes, as shown in Fig. 4. Below 550 K, the observed yields are close to those estimated based on the results with the 12 μm powder, consistent with the concept of a constant penetration thickness proposed by Yavor *et al.*[13]

Above 550 K, we observe a rapid increase in the hydrogen yield for the 55 μm and 120 μm powders that departs from that predicted by the penetration thicknesses obtained from the results for 12 μm powders below 475 K. The fit predicts maximum yields of 66% and 36% for the 55 μm and 120 μm powders, respectively, while we observe full hydrogen yield above 600 K for all powders.

3.2 Aluminum cans, slugs and plates

It is of practical interest to investigate the reaction yield of coarse aluminum materials, such as those that make up aluminum scrap and waste, under the highly reactive conditions identified in the previous section. Aluminum slugs measuring 3mm, 2-mm-thick aluminum
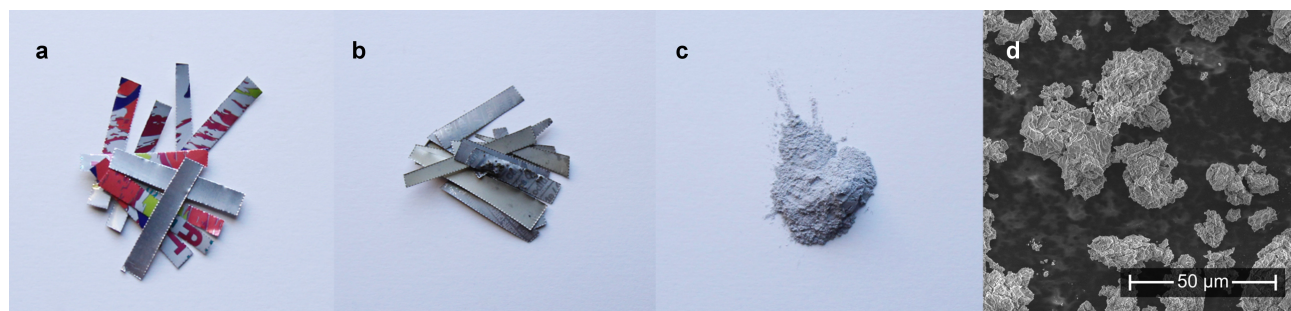
8

Figure 6: Images of the aluminum can before and after reaction with water. (a) Shredded aluminum can before experiment (b) Reaction products for experiment at 625 K (c) reaction products of aluminum can reacting with supercritical water (d) SEM image of reaction products of aluminum can reacting with supercritical water (500x magnification).
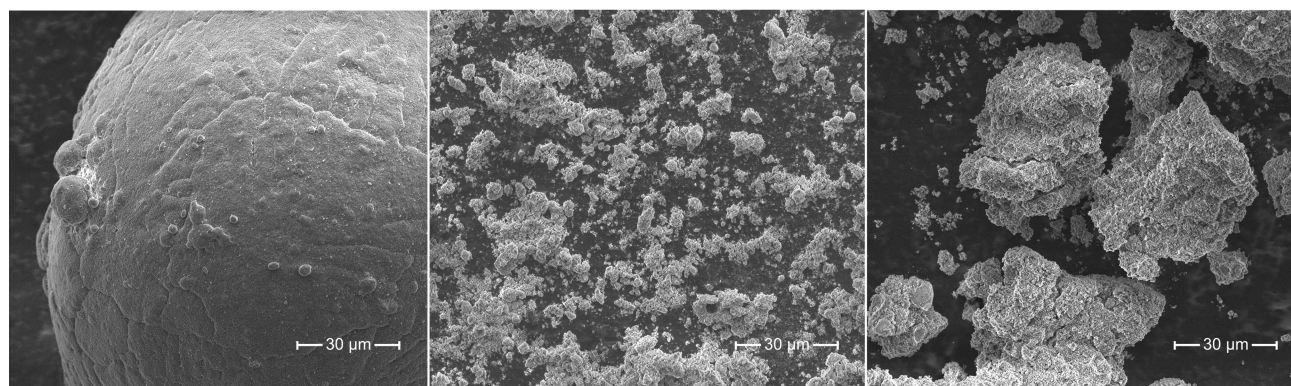

Figure 7: SEM of the 120 μm powder at 1000x magnification. (left) As received (center) Reaction products after experiment at 600 K (right) Reaction product after exposure to supercritical water. The yield in both the subcritical and the supercritical experiments was 100%. Reaction products from the subcritical experiment are a fine powder, with particles on the order of 2-3 μm, with the presence of some agglomerates. The supercritical products are agglomerates of approximately 30 μm.

plates, and shredded aluminum cans are used to represent the coarse materials that could be processed with an aluminum-water reactor.

As illustrated in Fig. 5, below 550 K there is virtually no hydrogen yield for the aluminum slugs or plates. Above this temperature, the yield increases with temperature in the case of the aluminum slugs, plate, and the stripped aluminum can. In the case of the unmodified shredded aluminum can, there is no hydrogen production until the supercritical regime is reached. In all cases, full yield is achieved once the critical temperature of 647 K is reached.

The difference in yield of the stripped aluminum can vs. the unmodified can at 625 K is due to the presence of an anti-corrosion polymer coating used on beverage containers. This coating stays intact in subcritical water but is compromised in supercritical water because of the ability of supercritical water to dissolve non-polar organic species. This quality of supercritical water has already been exploited for use in waste management.[47] In our experiment, we believe the supercritical water dissolved the coating, thereby exposing the aluminum can to the supercritical fluid allowing for the full oxidation of the aluminum can.

3.3 Reaction in sub- and super-critical water

In Fig. 6a, unreacted shredded aluminum from the unmodified common aluminum can is shown. The next panel, Fig. 6b, shows the reaction products of an experiment where the unmodified aluminum can was exposed to 625 K water for over 20 minutes. There was no hydrogen production or visible change in the appearance of the metal. The reaction products of the experiment where the aluminum can was exposed to supercritical water for the same amount of time are shown in Fig. 6c. In the supercritical experiment, 100% hydrogen yield was achieved. The significant increase in yield observed for the coarsest particles near the critical point suggests a change in the reaction mechanism. This newly observed reaction mechanism could open the door to high-efficiency oxidation of coarse aluminum materials and scrap.

The reaction products of the common aluminum can in supercritical water, as shown by the SEM image in Fig. 6d, are a very fine powder with particles on the nanometric scale which formed micrometric agglomerates. Since no reaction was observed with the aluminum can in subcritical water, we look to the results of the 120 μm powder to better understand the nature of the reaction products formed. Full oxidation using the 120 μm powder was reached at 600 K and at 650 K (see Fig. 4). SEM images of these reaction products are shown in Fig. 7. Supercritical water is a non-polar fluid and can dissolve substances, such as aluminum hydroxide, that are otherwise immiscible in subcritical water;[48] therefore it was expected that the products of the supercritical experiments would be a finer hydroxide product than those formed in the subcritical experiments. Instead, we observed that the subcritical products have particles sized approximately 2–3 μm whereas the supercritical products consist of agglomerates approximately ten times larger, the same scale as the supercritical aluminum can reaction products (*cf.* Fig. 6d). Our findings are consistent with those of previous studies,[49] which used different reactants, but showed oxides formed under supercritical conditions consist of crystals which are larger than those formed in subcritical water. XRD analysis of the products, included as Fig. 8, indicate that, in both cases, the product is boehmite (AlO(OH)) and the degree of crystallinity is above 85%.

4 Discussion

Up to 525 K, estimated yield are similar to the predictions of Yavor *et al.* regarding penetration thickness, as shown in Fig. 4. Above this temperature there is a marked improvement to reaction efficiency which cannot be explained by the increase in temperature alone. If temperature were the only relevant variable, the yield would follow the dashed line in Figs. 4 and 5; instead, the yield is much higher. We believe that the key to the enhanced reaction efficiency at temperatures above 525 K observed in this study is in the change in the ionic product of water.

The ionic product reaches a maximum around 573 K before dropping sharply and then monotonically decreasing after the critical point.[49] The high ionic product corresponds to a fluid that is high in H^+ and OH^- ions. The OH^- ions are a more mobile species and are able to exploit any porosity in formed hydroxides to electrochemically react with the aluminum metal.[27,28] At the same time, the H^+ protons are reduced forming hydrogen gas.[28] The high density of H^+ and OH^- ions effectively furnish the fluid with the ability to act as a self-
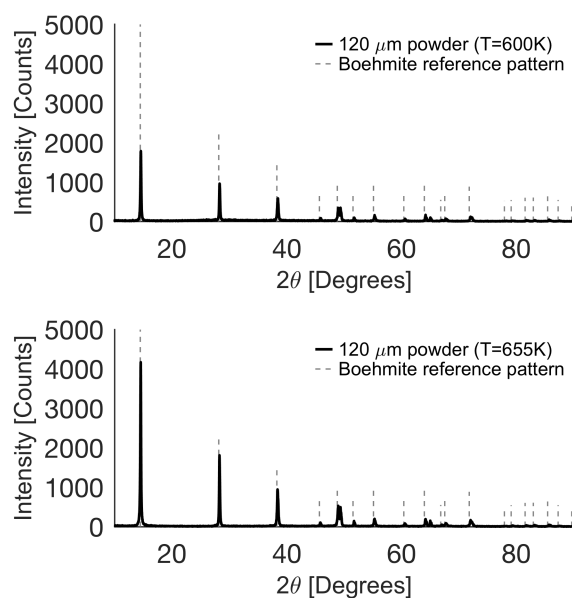
10

Figure 8: XRD analysis results of 120 μm powder reaction products. (top) Reaction products after experiment at 600 K (bottom) Reaction product after exposure to supercritical water. Both patterns show similar degrees of crystallinity and the resulting product in both cases is boehmite (AlOOH).

neutralizing acid-base catalyst.[50] Both acid and base catalysts have been shown to increase reaction rates.[27,33–35,50] The ionic product also increases rates of hydrolysis which improves yields,[49] even before the supercritical regime is reached. The net effect of these changes is exhibited in the data shown in Figs. 4 and 5.

As the temperature of liquid water increases, relative permittivity, the property governing solvent behaviour, decreases. Under normal conditions, the relative permittivity of liquid water is around 80 because of the preferred dipole orientation of water.[51] In supercritical water, this value ranges from 1–10, depending on pressure.[48] The low relative permittivity of the supercritical fluid means that water is no longer polar and the miscibility of non-polar solutes increases. In aluminum-water reactions, this means that the oxides formed in the reaction are unable to offer any passivation to the bulk aluminum beneath, thereby allowing for the full oxidation of large particles. In sub-critical water, it is this passivation mechanism which prevents complete oxidation.

The viscosity of water, the property which controls the transport properties of liquid water, also decreases as temperature increases. Under supercritical conditions, the viscosity of water is approximately 10% of the viscosity of liquid water under normal conditions. The low viscosity promotes mass transfer and diffusion of solutes in supercritical fluid.[51] The result is an enhancement of diffusion-controlled chemical reactions, such as the aluminum-water reaction.

11

5   Conclusions

The use of high-pressure and high-temperature sub- and super-critical water creates an efficient regime for the oxidation of a wide range of aluminum particles, including coarse materials and common aluminum alloys. It was previously believed that the hydroxides formed on the surface of the particle would prevent complete oxidation of larger particles, however, we have demonstrated 100 % hydrogen yield is possible in aluminum particles up to 3 mm.

A distinct change in reaction efficiency was observed around 550 K with the 55 µm and 120 µm powders, while the 12 µm powder followed the curve predicted by earlier work. Up to this temperature, the 3 mm aluminum slugs and 2 mm plate had yields close to zero, above this temperature the yields increased with temperature. We attribute the significant change in reaction efficiency and product morphology to the high ionic product of water at these temperatures and pressures. The high ionic product corresponds to a fluid rich in OH^- ions, which, it has been shown, are an effective catalyst for the aluminum-water reaction.

Under supercritical conditions, 100 % hydrogen yield was achieved in all materials tested. Supercritical water proved to be particularly effective in oxidizing the aluminum can. All experiments in the sub-critical regime using the as-received soda can resulted in zero hydrogen yield. The stripped soda can had a yield of approximate 20 % at 625 K. In both cases, full hydrogen yield was achieved in supercritical water at 650 K. Supercritical water has a low relative permittivity and viscosity which, when combined, create an environment highly conducive to oxidation.

Aluminum-water reactions are a promising avenue for converting renewable energy stored in aluminum into heat and hydrogen for use in a variety of power applications. These findings indicate that the use of high-temperature, high-pressure water creates an efficient reaction regime for coarse aluminum materials.

Conflicts of interest

There are no conflicts to declare.

Acknowledgements

References

[1] K. A. Trowell, J. M. Bergthorson, S. Goroshin and D. L. Frost, *Applied Energy*, 2020, **275**, 1–8.

[2] J. M. Bergthorson, *Progress in Energy and Combustion Science*, 2018, **68**, 169–196.

[3] E. Balomenos, D. Panias and I. Paspaliaris, *Mineral Processing and Extractive Metallurgy Review*, 2011, **32**, 69–89.

[4] A. Allanore, *Electrochimica Acta*, 2013, **110**, 587–592.

[5] T. R. Beck, *JOM*, 2013, **65**, 267–271.

[6] International Energy Agency, *Tracking Industry*, 2019, https://www.iea.org/reports/tracking-industry-2019/aluminium.

[7] A. Buttler and H. Spliethoff, *Renewable and Sustainable Energy Reviews*, 2018, **82**, 2440–2454.

[8] M. Gardiner and S. Satyapal, *Energy requirements for hydrogen gas compression and liquefaction as related to vehicle storage needs*, Depoartment of energy technical report, 2009.

[9] J. Bergthorson, S. Goroshin, M. Soo, P. Julien, J. Palecka, D. Frost and D. Jarvis, *Applied Energy*, 2015, **160**, 368–382.

[10] J. M. Bergthorson, Y. Yavor, J. Palecka, W. Georges, M. Soo, J. Vickery, S. Goroshin, D. L. Frost and A. J. Higgins, *Applied Energy*, 2017, **186**, 13–27.

[11] E. I. Shkolnikov, A. Z. Zhuk and M. S. Vlaskin, *Renewable and Sustainable Energy Reviews*, 2011, **15**, 4611–4623.

[12] A. Steinfeld, P. Kuhn, A. Reller, R. Palumbo, J. Murray and Y. Tamaura, *International Journal of Hydrogen Energy*, 1998, **23**, 767–774.

[13] Y. Yavor, S. Goroshin, J. M. Bergthorson, D. L. Frost, R. Stowe and S. Ringuette, *International Journal of Hydrogen Energy*, 2013, **38**, 14992–15002.

[14] Y. Yavor, S. Goroshin, J. M. Bergthorson and D. L. Frost, *International Journal of Hydrogen Energy*, 2015, **40**, 1026–1036.

[15] H. Z. Wang, D. Y. C. Leung, M. K. H. Leung and M. Ni, *Renewable and Sustainable Energy Reviews*, 2009, **13**, 845–853.

[16] C. R. Jung, A. Kundu, B. Ku, J. H. Gil, H. R. Lee and J. H. Jang, *Journal of power Sources*, 2008, **175**, 490–494.

[17] E. Shkolnikov, M. Vlaskin, A. Iljukhin, A. Zhuk and A. Sheindlin, *Journal of Power Sources*, 2008, **185**, 967–972.

[18] A. Gany, S. Elitzur and V. Rosenband, *Journal of Shipping and Ocean Engineering*, 2015, **5**, 151–158.

[19] F. Franzoni, M. Milani, L. Montorsi and V. Golovitchev, *International Journal of Hydrogen Energy*, 2010, **35**, 1548–1559.

[20] M. Vlaskin, E. Shkolnikov, A. Bersh, A. Zhuk, A. Lisicyn, A. Sorokovikov and Y. Pankina, *Journal of Power Sources*, 2011, **196**, 8828–8835.

[21] T. R. Sippel, T. L. Pourpoint and S. F. Son, *Propellants, Explosives, Pyrotechnics*, 2013, **38**, 56–66.

[22] G. A. Risha, T. L. Connell Jr., R. A. Yetter, D. S. Sundaram and V. Yang, *Journal of Propulsion and Power*, 2014, **30**, 133–142.

[23] J. P. Foote, B. R. Thompson and J. T. Lineberry, *Advances in Chemical Propulsion: Science to Technology*, Taylor & Francis Group, 2001, ch. Combustion, pp. 133–146.

[24] D. Barone, E. Loth, P. Weiss, B. Theobald and D. Parker, *AIAA Paper*, 2011, **5904**, 2011.

[25] M. N. Larichev, *Metal Nanopowders: Production, Characterization, and Energetic Applications*, Wiley-VCH Verlag GmbH & Co. KGaA, Weinheim, Germany, 2014, ch. Chapter 7:, pp. 163–198.

[26] J. Petrovic and G. Thomas, *Reaction of aluminum with water to produce hydrogen, a study of issues related to the use of aluminum for On-Board vehicular hydrogen storage*, Us department of energy technical report, US Department of Energy, 2010.

[27] W. Vedder and D. A. Vermilyea, *Transactions of the Faraday society*, 1969, **65**, 561–584.

[28] B. C. Bunker, G. C. Nelson, K. R. Zavadil, J. C. Barbour, F. D. Wall, J. P. Sullivan, C. F. Windisch, M. H. Engelhardt and D. R. Baer, *The Journal of Physical Chemistry B*, 2002, **106**, 4705–4713.

[29] M. Digne, P. Sautet, P. Raybaud, H. Toulhoat and E. Artacho, *The Journal of Physical Chemistry B*, 2002, **106**, 5155–5162.

[30] A. K. Narayana Swamy and E. Shafirovich, *Combustion and Flame*, 2014, **161**, 322–331.

[31] P. Godart, J. Fischman, K. Seto and D. Hart, *International Journal of Hydrogen Energy*, 2019, **44**, 11448–11458.

[32] W.-Z. Gai, W.-H. Liu, Z.-Y. Deng and J.-G. Zhou, *International Journal of Hydrogen Energy*, 2012, **37**, 13132–13140.

[33] Y. A. Aleksandrov, E. I. Tsyganova and A. L. Pisarev, *Russian Journal of General Chemistry*, 2003, **73**, 689–694.

[34] D. Stockburger, J. H. Stannard, B. M. L. Rao, W. Kobasz and C. D. Tuck, Proc Symp Hydrogen Storage Mater Batteries Electrochem, 1992, pp. 431–444.

[35] W. M. Carroll and C. B. Breslin, *Corrosion Science*, 1992, **33**, 1161–1177.

[36] V. Rosenband and A. Gany, *International Journal of Hydrogen Energy*, 2010, **35**, 10898–10904.

[37] S. Elitzur, V. Rosenband and A. Gany, *International Journal of Hydrogen Energy*, 2014, **39**, 6328–6334.

[38] A. V. Parmuzina and O. V. Kravchenko, *International Journal of Hydrogen Energy*, 2008, **33**, 3073–3076.

[39] A. A. Vostrikov, O. N. Fedyaeva, I. I. Fadeeva and M. Y. Sokol, *Russian Journal of Physical Chemistry B*, 2010, **4**, 1051–1060.

[40] E. Czech and T. Troczynski, *International Journal of Hydrogen Energy*, 2010, **35**, 1029–1037.

[41] B. Alinejad and K. Mahmoodi, *International Journal of Hydrogen Energy*, 2009, **34**, 7934–7938.

[42] K. Mahmoodi and B. Alinejad, *International Journal of Hydrogen Energy*, 2010, **35**, 5227–5232.

[43] M. Urbonavicius, S. Varnagiris and D. Milcius, *Energy Technology*, 2017, **5**, 2300–2308.

[44] M. Vlaskin, E. Shkolnikov and A. Bersh, *International Journal of Hydrogen Energy*, 2011, **36**, 6484–6495.

[45] P. Setiani, N. Watanabe, R. R. Sondari and N. Tsuchiya, *Materials for Renewable and Sustainable Energy*, 2018, **7**, 10.

[46] T. M. Seward and E. U. Franck, *Berichte der Bunsengesellschaft für physikalische Chemie*, 1981, **85**, 2–7.

[47] E. F. Gloyna, L. Li and R. N. McBrayer, *Water Science and Technology*, 1994, **30**, 1–10.

[48] G. Brunner, *Supercritical Fluid Science and Technology*, Elsevier, 2014, vol. 5, pp. 569–589.

[49] A. A. Galkin and V. V. Lunin, *Russian Chemical Reviews*, 2005, **74**, 21–35.

[50] D. K. Smith, D. K. Unruh, C.-C. Wu and M. L. Pantoya, *The Journal of Physical Chemistry C*, 2017, **121**, 23184–23191.

[51] H. H. Weingärtner and E. E. Franck, *Angewandte Chemie International Edition*, 2005, **44**, 2672–2692.